DeltaDeno: Zero-Shot Anomaly Generation via Delta-Denoising Attribution

Chaoran Xu Chengkan Lv Qiyu Chen Yunkang Cao Feng Zhang* Zhengtao Zhang Institute of Automation, Chinese Academy of Sciences

Abstract

Anomaly generation is often framed as few-shot fine-tuning with anomalous samples, which contradicts the scarcity that motivates generation and tends to overfit category priors. We tackle the setting where no real anomaly samples or training are available. We propose Delta-Denoising (**DeltaDeno**), a training-free zero-shot anomaly generation method that localizes and edits defects by contrasting two diffusion branches driven by a minimal prompt pair under a shared schedule. By accumulating per-step denoising deltas into an image-specific localization map, we obtain a mask to guide the latent inpainting during later diffusion steps and preserve the surrounding context while generating realistic local defects. To improve stability and control, DeltaDeno performs token-level prompt refinement that aligns shared content and strengthens anomaly tokens, and applies a spatial attention bias restricted to anomaly tokens in the predicted region. Experiments on public datasets show that DeltaDeno achieves great generation, realism and consistent gains in downstream detection performance. Code will be made publicly available.

1. Introduction

Automated visual inspection [2] is a cornerstone of modern smart manufacturing and safety-critical operations. In principle, high-performance anomaly detection (AD) systems can be trained with sufficient defective data under supervised learning [3, 7, 8, 28]. In practice, defects are rare, diverse, and costly to curate. Early-stage production lines and high-yield semiconductor processes exhibit exceptionally low defect rates. Many defects emerge only after process changes or tool aging and pixel-accurate masks also require expert annotation [13, 18, 34, 37]. Beyond scarcity, domains evolve over time through changes in materials, suppliers, and lighting, which creates persistent distribution shifts that degrade deployed AD [19]. These factors motivate *anomaly generation (AG)* as a complementary route to

provide realistic and controllable abnormal samples and to stress-test detectors without halting production [18, 33, 35].

Early AG efforts centered on cut-paste composition [23, 24, 35] and GAN-based generators [12, 36]. With the rapid advances in diffusion models [11, 16, 17, 27, 29], diffusion-based AG methods have since emerged and become a major line of work that are usually guided by masks, bounding boxes, or short text prompts [10, 31, 34]. This line of research is primarily driven by two objectives. The first is *realism* [19, 33], meaning that the generated region should be photometrically and geometrically consistent with the background. The second is *controllability* [31], meaning that one can specify where the change occurs, how strong it is, and what type of defect is inserted.

Despite steady progress, many current pipelines adopt few-shot anomaly generation (FSAG) [12, 18, 19, 31, 33]. A pretrained generator is adapted with a small number of real anomalous samples and masks, and the adapted model is then used to expand the training set. This practice runs against the motivation for AG, which is to reduce dependence on rare and costly annotations. In many deployments, anomalous samples do not exist at scale, are expensive to collect, or are restricted by safety and privacy rules. FSAG also binds the generator to category-specific priors such as texture, lighting, and geometry, which encourages overfitting and weakens transfer across categories. As a result, gains on category A often fail to carry over to category B without anomalous samples. Zero-shot anomaly generation (ZSAG) aims to remove this dependence on anomalous pixels and additional training. AnomalyAny [34] is a recent ZSAG example that shows good cross-category generalization, yet it also exposes practical limits. As shown in Fig. 1, DRAEM follows the cut-paste paradigm and shows strong generalization ability but very limited realism [35]. The representative FSAG approach, Anomaly Diffusion, relies on supervised fine-tuning with real anomalous samples and masks, which makes it difficult to generalize when no downstream anomalies are available [18]. AnomalyAny builds masks from attention maps, but their low resolution and inaccurate localization remain problematic.

To address these limitations, we present DeltaDeno, a

^{*}Corresponding author.

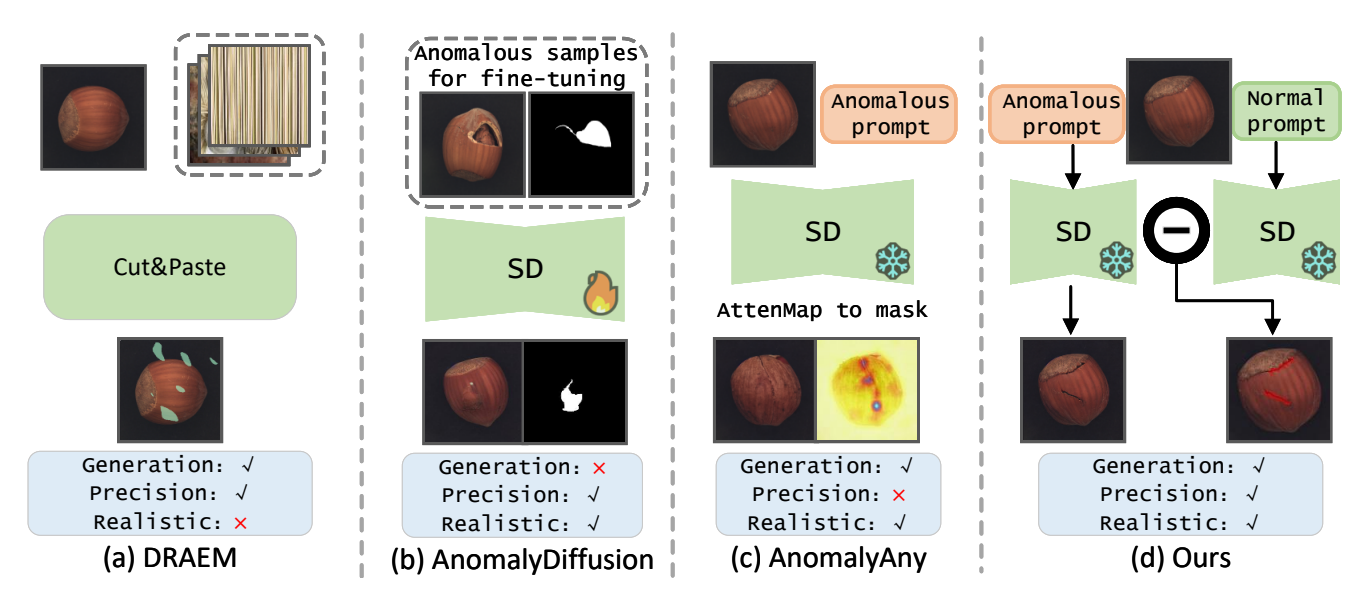


Figure 1. Comparison between visual anomaly generation methods. Compared with prior approaches, **DeltaDeno** delivers cross-category generalization, precise masks, and high realism while requiring no fine-tuning.

training-free ZSAG framework that localizes and generates defects without any anomalous samples or model adaptation. We use a minimal pair of prompts that differ only by an anomaly descriptor to drive two synchronized diffusion branches under the same schedule. At each step, we compare the two branches' denoiser predictions and accumulate their differences to build an image-specific anomaly attribution map as mask. Later, we perform mask-guided latent inpainting, which refines the initially coarse anomaly regions during later time-steps while preventing the synthesized defects from spilling into normal areas. We also apply normal-reference guided initialization, which starts from a partially noised encoding of the normal image to keep synthesis aligned with the original content distribution and to shorten the reverse trajectory. To further sharpen localization, we introduce lightweight token-level prompt refinement and spatial attention biasing, which strengthen the anomaly-token discrepancy across the two denoising branches and suppress the influence of non-anomaly tokens, yielding a more precise mask with fewer spurious edits. This attribution-guided design ties localization to the model's own denoising dynamics and produces sharper, more realistic anomalies without fine-tuning. The main contribution of this paper can be summarized as follows:

- We propose a zero-shot, training-free anomaly generation framework DeltaDeno that requires no anomalous samples, no fine-tuning, and no task-specific retraining.
- We introduce delta-denoising attribution for ZSAG, using stepwise denoising discrepancies between normal and anomaly prompts to localize and generate defects, while lightweight prompt refinement and spatial attention biasing improve realism and mask precision.

 We demonstrate strong localization fidelity, photorealism, and cross-category generalization across industrial and other domains, yielding competitive improvements in downstream AD performance.

2. Related Work

2.1. Diffusion-based Image Editing

Text-guided diffusion enables high-quality and widecoverage image editing, with Stable Diffusion [29] and its latent variants serving as scalable backbones for reconstruction and control. Some methods focus on preserving structural consistency while steering appearance. For example, SDEdit [25] adjusts denoising schedules to balance fidelity and edit strength, while Prompt-to-Prompt [15] constrains cross-attention so that edits follow token semantics without disturbing the spatial layout. Attend-and-Excite [6] further amplifies weak tokens to improve semantic faithfulness. Other approaches enhance localization by tightening the reconstruction path, as in Null-text inversion [26] and Imagic [20], or by confining edits with masks as demonstrated in blended latent diffusion [1]. DiffEdit [9] derives an edit mask by contrasting source and target prompts under a shared schedule, while subsequent methods such as MasaCtrl [5] and InstructPix2Pix [4] extend diffusion control to multi-prompt and instruction-driven editing. Inspired by these works, we edit normal images with anomaly semantics, enabling training-free, context-consistent anomaly generation.

2.2. Anomaly Generation

Anomaly generation provides synthetic abnormal samples for training, evaluation, and stress testing of anomaly detection systems. Early practical approaches rely on cutpaste composition, such as DRAEM, which transfers defect patches onto normal images but often suffers from lighting and material inconsistency [35]. GAN-based AG [12, 36] improves texture realism and diversity through adversarial learning, while diffusion-based backbones further enhance fidelity and controllability by introducing masks, boxes, or text prompts to guide synthesis. A common trend is FSAG [10, 18, 19], which fine-tunes a pretrained generator on a small set of real anomalies and pixel masks to expand training data. Although FSAG produces detailed and category-specific defects, it depends on scarce annotations and tends to overfit to class priors, limiting cross-domain generalization. To remove this dependence, ZSAG leverages the intrinsic guidance of pretrained diffusion models and text prompts. Recent ZSAG methods, such as AnomalyAny [34], broaden category coverage but often yield coarse attention-derived masks and require slow iterative inference. In contrast, we aggregate step-wise denoising discrepancies between normal and anomaly prompts to directly attribute semantic divergence, enabling train-free, high-quality local anomaly generation with matched mask.

3. Method

We present DeltaDeno, a training-free zero-shot anomaly generation framework that localizes and generates defects through delta-denoising attribution, without any anomalous pixel labels or model adaptation, as shown in Fig. 2. We contrast the denoiser predictions of two synchronized diffusion branches, driven by normal and anomaly prompts, to capture semantic divergences as anomaly masks. We then refine these coarse regions via mask-guided latent inpainting, preserving contextual consistency and preventing spill-over into clean areas. To maintain alignment with the normal content distribution, we apply normal reference guided initialization, which starts from a partially noised normal encoding and shortens the reverse trajectory. Furthermore, lightweight token-level prompt refinement and spatial attention biasing sharpen localization by emphasizing anomaly-related tokens and suppressing irrelevant ones.

3.1. Preliminaries

Latent diffusion models. Denoising diffusion models learn the data distribution by predicting the noise added at each step. We follow latent diffusion, where an encoder \mathcal{E} maps an image x to a latent $z_0 = \mathcal{E}(x)$ and a decoder \mathcal{D} reconstructs images from latents [21]. Given a noise $\epsilon \sim \mathcal{N}(0, \mathbf{I})$

and a scheduler with (α_t, σ_t) , the noisy latent is

$$z_t = \alpha_t z_0 + \sigma_t \epsilon. \tag{1}$$

A U-Net [30] ϵ_{θ} predicts the added noise at step t, and the training objective of LDM is

$$\mathcal{L}_{\text{LDM}} = \mathbb{E}_{z_0 = \mathcal{E}(x), \, \epsilon \sim \mathcal{N}(0, \mathbf{I}), \, t} \left[\| \epsilon - \epsilon_{\theta}(z_t, t) \|_2^2 \right]. \quad (2)$$

At inference, the reverse process starts from $z_T \sim \mathcal{N}(0, \mathbf{I})$ and gradually denoises to z_0 , followed by $x' = \mathcal{D}(z_0)$.

Cross-Attention in U-Net. Let $E \in \mathbb{R}^{Z \times d}$ be the text token embeddings (with Z tokens) and $F^l \in \mathbb{R}^{N \times d}$ be the flattened image features at layer l (with $N = r^2$ image tokens). For a cross-attention in U-Net, the projections are

$$Q^{l} = F^{l}W_{q}^{(l)}, \qquad K^{l} = EW_{k}^{(l)},$$
 (3)

and the cross-attention map is

$$A^{l} = \operatorname{softmax}\left(\frac{Q^{l}(K^{l})^{\top}}{\sqrt{d_{h}}}\right) \in \mathbb{R}^{N \times Z},$$
 (4)

where $A^l \in \mathbb{R}^{N \times Z}$ represents the attention weights from all N image tokens to the Z text tokens.

Latent inpainting. For localized edits and background preservation, inference often blends a proposed edited latent \tilde{z}_{t-1} with a source latent z_{t-1}^{src} using a spatial mask $M \in [0,1]^{H_z \times W_z}$ at the latent resolution:

$$z_{t-1} = M \odot \tilde{z}_{t-1} + (1 - M) \odot z_{t-1}^{\text{src}}.$$
 (5)

This confines changes to the masked region while keeping the outside region consistent with the source.

3.2. Delta-Denoising Localization

Normal reference guided initialization. To ensure that the synthesized defective images do not deviate completely from the distribution of the original normal samples, we do not start the generation from pure Gaussian noise. We encode the guidance image $x^{\rm normal}$ to $z_0^{\rm normal}$ and partially noise it to an intermediate level $t_{\rm start}$:

$$z_{t_{\mathrm{start}}}^{\mathrm{normal}} = \sqrt{\bar{\alpha}_{t_{\mathrm{start}}}} z_0^{\mathrm{normal}} + \sqrt{1 - \bar{\alpha}_{t_{\mathrm{start}}}} \epsilon,$$
 (6)

where $t_{\rm start} = \gamma T$ and $\epsilon \sim \mathcal{N}(0,I)$. Sampling then starts from $t_{\rm start}$ and performs the remaining reverse steps $(t_{\rm start} \to 0)$ for both branches under the same schedule. This warm start preserves geometry and illumination, reduces computational cost, and prevents the class-typical drift observed when starting from pure noise.

Prompt design. We use a minimal pair of prompts that differ only by an anomalous attribute. For example, the *normal prompt* is `a photo of a {object}'', and the *anomaly prompt* is `a photo of a {object}

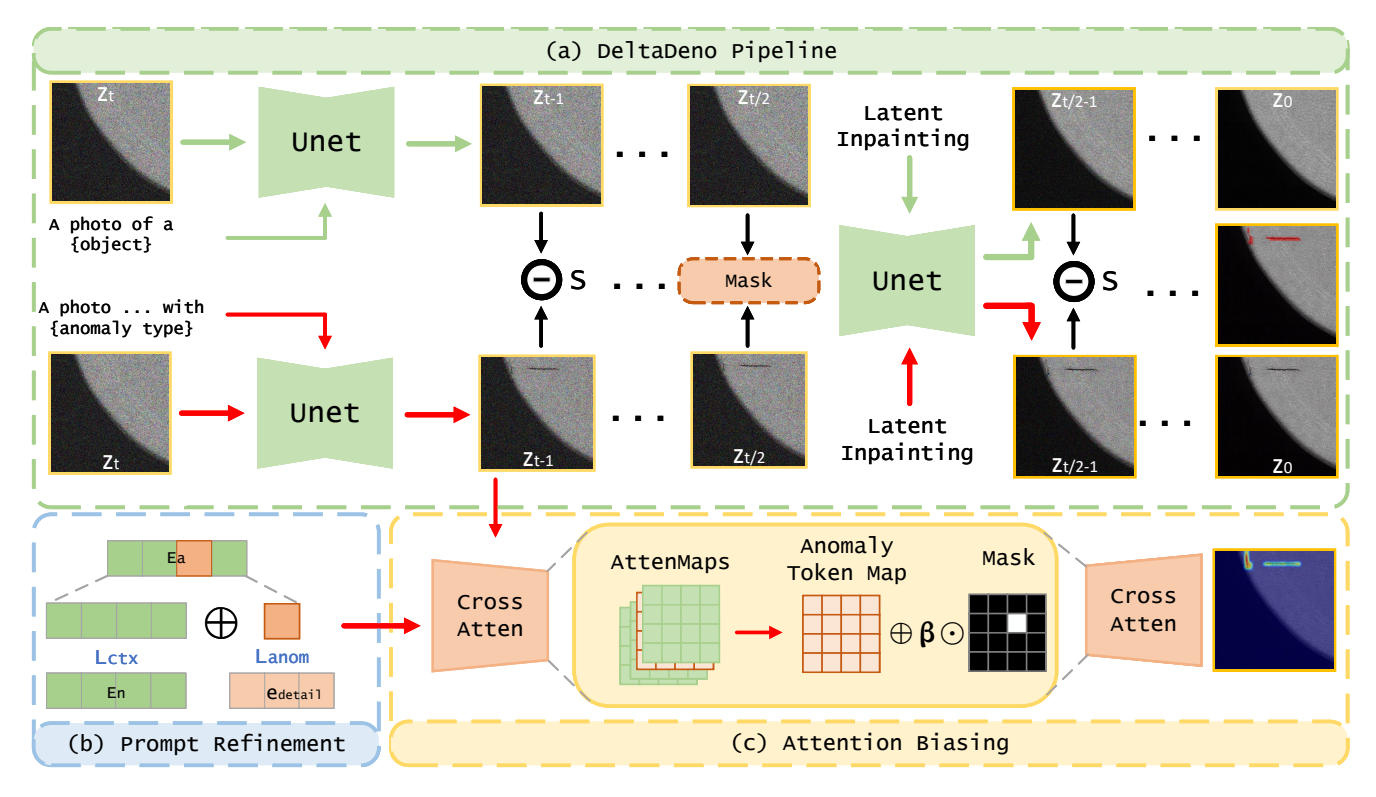


Figure 2. Overview of the DeltaDeno framework integrating delta-denoising localization, prompt refinement, and attention biasing.

with {anomaly type}''. Additionally, a *description prompt* is introduced for the anomaly token, which provides a refined semantic embedding (e.g., adding shape or intensity cues) during the subsequent prompt refinement stage. This descriptor is not inserted into the sentence but distilled into the anomaly token to enhance its representation to minimize off-target semantic drift.

Synchronized denoising and delta-attribution. Let T be the total number of inference steps. We define $t \in [T, T/2]$ as the early denoising stage and $t \in [T/2, 0]$ as the late denoising stage. We run two synchronized trajectories under the same schedule and guidance: a normal branch with prompt $p_{\rm n}$ and an anomaly branch with $p_{\rm a}$. Denote their latents at step t by $z_t^{\rm (n)}$ and $z_t^{\rm (a)} \in \mathbb{R}^{H_z \times W_z \times C}$. A single reverse step of the U-Net is

$$z_{t-1}^{(\cdot)} = \Phi(z_t^{(\cdot)}, \hat{\epsilon}_{\text{cfg}}(z_t^{(\cdot)}, t, e_{(\cdot)}), t), \tag{7}$$

where Φ is the reverse-step operator, $\hat{\epsilon}_{\rm cfg}$ is the classifier-free guided prediction, and $e_{(\cdot)}$ is the text embedding of $p_{\rm n}$ or $p_{\rm a}$. We measure the per-step discrepancy between the two branches after each reverse update:

$$d_{t-1}(u) = \left\| z_{t-1}^{(n)}(u) - z_{t-1}^{(a)}(u) \right\|_{2}, \tag{8}$$

where u indexes a spatial position in the latent feature map, and the ℓ_2 norm is applied over channels. The accumulator

integrates the discrepancies along the reverse trajectory as

$$S_{t-1}(u) = S_t(u) + d_{t-1}(u), S_{t_{\text{ctart}}}(u) = 0, (9)$$

where $t_{\rm start}$ denotes the starting timestep. At the $t_{\rm mid} = \lfloor T/2 \rfloor$, we lightly smooth and normalize $S_{t_{\rm mid}}$ to obtain a continuous delta map \hat{S} , and threshold it to generate a binary mask:

$$M_{\text{mid}}(u) = \mathbf{1} \left\{ \hat{S}(u) > \tau_{\text{mid}} \right\}. \tag{10}$$

After extracting $M_{\rm mid}$, the accumulator S is reset to zero, and a new aggregation begins for the late denoising stage, focusing on boundary refinement and local details.

During the late denoising stage, the image-specific mask $M_{
m mid}$ serves as a latent inpainting mask that confines subsequent edits to the coarse anomaly region discovered earlier. The update is

$$z_{t-1} \leftarrow M_{\text{mid}} \odot \tilde{z}_{t-1} + (1 - M_{\text{mid}}) \odot z_{t-1}^{\text{src}}, \tag{11}$$

where the $z_{t-1}^{\rm src}$ is obtained by forward noising the normal reference latent $z_0^{\rm normal}$ to the same timestep via DDIM [32]. This operation refines defect synthesis inside the mask while preserving the normal-image distribution outside, ensuring local detail enhancement and global consistency.

3.3. Prompt Refinement and Attention Biasing

Diffusion-based generation in Stable Diffusion is tightly coupled with the text condition, where each token dynamically interacts with visual features throughout the denoising process. Given our delta-denoising formulation, the semantic discrepancy between the two diffusion branches should be localized exclusively to the anomaly token, rather than spreading across the entire prompt. Therefore, we introduce two complementary mechanisms, *Token-level prompt refinement* and *Spatially-biased cross-attention*.

Token-level prompt refinement. To convey fine-grained defect semantics while minimizing semantic differences outside the anomaly token, we perform a lightweight token-level refinement on the anomaly prompt embedding before denoising. Let the normal and anomaly prompts be tokenized as $E_{\rm n}=\{e_{\rm n}^1,\ldots,e_{\rm n}^{Z_{\rm n}}\}$ and $E_{\rm a}=\{e_{\rm a}^1,\ldots,e_{\rm a}^{Z_{\rm a}}\}$, respectively. We selectively update $E_{\rm a}$ with two complementary objectives.

(i) Anomaly Semantic Distillation. Embeddings of anomaly-specific tokens (e.g., crack, scratch, damage) are steered toward a detailed semantic anchor $e_{\rm detail}$ distilled from a more descriptive phrase:

$$\mathcal{L}_{\text{anom}} = 1 - \cos(e_a^j, e_{\text{detail}}) + \lambda ||e_a^j - e_{\text{detail}}||_2^2.$$

(ii) Context Alignment for non-anomaly tokens. For the remaining Z' non-anomaly tokens in the anomaly prompt, we compute their mean embedding as a context centroid and encourage each token to stay close to it:

$$ar{e}_{ ext{ctx}} = rac{1}{Z'} \sum_{j=1}^{Z'} e_{ ext{a}}^{j}, \qquad \mathcal{L}_{ ext{ctx}} = rac{1}{Z'} \sum_{j=1}^{Z'} \|e_{ ext{a}}^{j} - ar{e}_{ ext{ctx}}\|_{2}^{2}.$$

This simple MSE regularization stabilizes the shared context and prevents semantic drift among non-anomaly tokens. We jointly optimize the two objectives as

$$\mathcal{L}_{prompt} = \mathcal{L}_{anom} + \eta \, \mathcal{L}_{ctx},$$

and update the anomaly prompt embedding as

$$E_{\rm a} \leftarrow E_{\rm a} - \alpha_t \nabla_{E_{\rm a}} \mathcal{L}_{\rm prompt},$$
 (12)

where α_t is the step size and η balances the two objectives. This training-free refinement runs for a few iterations with a fixed step size, ensuring that semantic changes remain localized to the anomaly token while other tokens retain the original context.

Spatially-biased cross-attention. We use a two-stage spatial prior for attention. During the early denoising stage, a coarse foreground mask $M_{\rm fg}$ (from SAM [22]) activates plausible surface regions. During the late denoising stage, we switch to the $M_{\rm mid}$ from Sec. 3.2 to focus the defect

Algorithm 1 DeltaDeno Inference

```
1: M_{\mathrm{fg}} \leftarrow \mathrm{SAM}(I), z_0 \leftarrow \mathrm{VAE\text{-}enc}(I),
    normal reference guided(z_0)
 2: Token-level prompt refinement for p_a
 3: Run two diffusion branches with same schedule and
     seed: (p_n, p_a)
 4: for each step t do
       if early denoising stage then
 5:
          attention biasing with M_{\rm fg}; update S
 6:
 7:
       else if t_{\rm mid} then
 8:
          M_{\text{mid}} \leftarrow \text{threshold}(\text{clean}(\text{normalize}(S))); \text{ reset } S
 9:
          attention biasing and latent inpainting with M_{\rm mid};
10:
11:
       end if
12: end for
13: M
                    threshold(clean(normalize(S))), I'
     VAE-dec(anomaly branch)
14: return (I', M)
```

area. At each step, we inject the mask M into the cross-attention logits for the anomaly token only:

$$A^{l} = \operatorname{softmax}\left(\frac{Q^{l}(K^{l})^{\top} + \beta M o_{a}^{\top}}{\sqrt{d_{h}}}\right), \qquad (13)$$

Here M represents the current spatial prior mask, either $M_{\rm fg}$ in the early denoising stage or $M_{\rm mid}$ in the late denoising stage, and o_a denotes the one-hot column selector that specifies the anomaly token $j{=}a$. The bias term $\beta\,M\,o_a^{\rm T}$ injects spatial awareness into the anomaly token's attention map, so that the model focuses on masked regions when attending to the anomaly description, while leaving other tokens unaffected to maintain overall consistency.

3.4. Inference

At inference, ZSAG generates a realistic defect image and its mask from a single normal input. Given a normal image I, a normal prompt $p_{\rm n}$, and an anomaly prompt $p_{\rm a}$, we: (i) run Token-level prompt refinement for $p_{\rm a}$ (ii) encode I into latent z_0 and get normal reference guided initialization to two synchronized diffusion branches conditioned on $p_{\rm n}$ and $p_{\rm a}$; (iii) accumulate latent discrepancies S during the early denoising stage to form $M_{\rm mid}$ and reset S at $t_{\rm mid}$; (iv) continue the late denoising stage with attention biasing and inpainting guided by $M_{\rm mid}$; (v) at the final step, re-threshold S to get the final mask M, and decode the anomaly branch as the defect image I'.

Table 1. Comparison with existing anomaly generation methods on generation quality and diversity.

Category	Crop-	Paste [24]	DFM	GAN [12]	Anom	alyDiff [18]	Anom	alyAny [34]	Ours		
	IS↑	IC-L↑	IS ↑	IC-L↑	IS ↑	IC-L↑	IS ↑	IC-L↑	IS ↑	IC-L↑	
bottle	1.43	0.04	1.62	0.12	1.58	0.19	1.73	0.17	2.36	0.27	
cable	1.74	0.25	1.96	0.25	2.13	0.41	2.06	0.41	2.49	0.41	
capsule	1.23	0.05	1.59	0.11	1.59	0.21	2.16	0.23	1.82	0.23	
carpet	1.17	0.11	1.23	0.13	1.16	0.24	1.10	0.34	1.27	0.45	
grid	2.00	0.12	1.97	0.13	2.04	0.44	2.31	0.38	2.26	0.39	
hazelnut	1.74	0.21	1.93	0.24	2.13	0.31	2.55	0.32	2.62	0.38	
leather	1.47	0.14	2.06	0.17	1.94	0.41	2.26	0.41	1.77	0.44	
metal_nut	1.56	0.15	1.49	0.32	1.96	0.30	1.82	0.27	2.00	0.31	
pill	1.49	0.11	1.63	0.16	1.61	0.26	2.91	0.30	2.26	0.33	
screw	1.12	0.16	1.12	0.14	1.28	0.30	1.33	0.32	1.29	0.37	
tile	1.83	0.20	2.39	0.22	2.54	0.55	2.66	0.53	2.08	0.49	
toothbrush	1.30	0.08	1.82	0.18	1.68	0.21	1.64	0.22	1.99	0.24	
transistor	1.39	0.15	1.64	0.25	1.57	0.34	1.66	0.28	1.97	0.32	
wood	1.95	0.23	2.12	0.35	2.33	0.37	1.93	0.41	2.19	0.44	
zipper	1.23	0.11	1.29	0.27	1.39	0.25	2.14	0.33	2.09	0.37	
Avg.	1.51	0.14	1.72	0.20	1.80	0.32	2.02	0.33	2.03	0.36	

Table 2. Comparison of downstream detection performance by training a U-Net on the generated data from different AG methods. Bold numbers indicate the best results among ZSAG methods.

	Few-shot Methods								Zero-shot Methods											
Category	DFM	IGAN	(AAAI'	23)	And	Diff (AAAI'2	24)	And	Gen (I	ECCV'	24)	Ano	Any (CVPR'	25)		Ου	ırs	
	$\overline{AUC_i}$	AP_i	AUC_p	AP_p	AUC_i	AP_i	AUC_p	AP_p	AUC_i	AP_i	AUC_p	AP_p	AUC_i	AP_i	AUC_p	AP_p	$ AUC_i $	AP_i	AUC_p	AP_p
bottle	63.9	83.8	55.2	7.01	97.7	99.3	94.6	81.6	96.6	98.8	75.6	57.4	94.9	98.0	86.9	32.2	97.2	98.8	86.0	28.4
cable	88.2	89.6	73.8	38.6	99.5	99.5	93.2	74.2	95.8	97.0	81.2	57.5	44.1	49.0	82.2	11.1	70.9	74.9	76.2	8.0
capsule	61.1	85.9	45.2	2.45	77.4	94.3	74.8	12.6	78.9	94.0	62.9	19.4	59.4	84.6	78.2	7.4	54.9	79.0	87.9	5.8
carpet	87.2	95.4	70.2	36.9	64.8	79.4	79.8	17.8	90.0	96.6	62.7	48.2	79.4	90.2	80.9	30.9	85.9	94.0	90.1	41.7
grid	53.2	68.3	64.7	7.29	97.4	98.9	89.8	32.2	96.0	98.0	71.8	29.5	85.7	92.7	73.9	5.3	81.3	89.9	77.3	8.7
hazelnut	99.7	99.8	93.3	82.8	95.9	97.5	88.5	70.0	98.0	98.0	92.7	61.6	98.8	99.0	95.3	43.8	99.1	99.2	97.5	69.6
leather	65.3	83.4	58.8	6.05	99.1	99.7	91.9	65.9	100.0	100.0	82.4	60.1	92.6	97.0	94.1	45.0	96.5	98.3	94.6	47.1
metal_nut	90.6	97.5	96.0	92.0	99.8	99.9	98.7	96.4	99.5	99.9	98.3	89.1	54.3	80.9	77.1	41.0	73.8	90.0	83.2	38.5
pill	87.0	96.9	91.2	73.5	93.2	98.6	94.9	79.3	97.5	99.4	96.4	78.9	65.9	88.9	88.9	36.7	89.7	97.3	93.3	65.1
screw	74.6	89.0	29.3	3.31	12.5	53.7	56.8	1.71	37.3	69.1	63.7	7.70	60.9	75.7	92.1	2.3	73.3	85.8	95.6	4.7
tile	100.0	100.0	97.9	94.2	100.0	100.0	96.6	91.0	100.0	100.0	90.9	72.0	97.0	98.5	89.2	53.9	99.9	100.0	87.0	51.9
toothbrush	95.8	98.2	67.8	30.1	95.8	98.2	73.2	27.9	93.6	97.0	60.6	22.5	89.6	95.0	75.2	12.2	89.2	94.1	78.9	12.9
transistor	79.2	76.3	45.2	8.47	99.9	99.8	94.3	81.2	98.5	95.8	66.0	38.6	78.9	72.4	65.2	12.0	78.8	76.8	58.9	14.9
wood	72.2	87.4	73.7	21.5	98.6	99.4	94.6	75.7	99.5	99.8	86.9	68.1	99.4	99.7	84.4	42.1	99.0	99.6	80.7	42.2
zipper	66.0	84.6	47.5	2.00	100.0	100.0	89.5	68.5		99.9	58.2	39.8	63.6	84.8	85.7	21.8	80.8	91.7	86.8	18.5
Mean	78.9	88.9	67.3	33.7	88.8	94.5	87.4	58.4	92.0	96.3	76.7	50.0	77.6	87.1	83.3	26.5	84.7	91.3	84.9	30.5

4. Experiments

4.1. Experiment Setup

Datasets and Baselines. Following the latest representative ZSAG and FSAG methods [10, 19, 33], we mainly conduct experiments on the widely used MVTec AD [2] dataset and results on other datasets are provided in the appendix. MVTec AD contains 15 object categories and 73 anomaly types, providing a comprehensive benchmark for both generation and localization. We compare with some existing few-shot and zero-shot methods including DRAEM [35], Crop-Paste [24], DFMGAN [12], AnomalyDiffusion [18], AnoGen [14], and AnomalyAny [34].

Evaluation Metrics. To quantitatively evaluate the

anomaly generation quality, we employ the Inception Score (IS) to assess image realism and the intra-cluster pairwise LPIPS distance (IC-LPIPS) to measure generation diversity. Following previous FSAG and ZSAG works, we also validate the usefulness of our generated anomalies by testing their effectiveness in anomaly detection frameworks. For anomaly localization and detection performance, we report both image-level and pixel-level metrics, including the Area Under the Receiver Operating Characteristic (AUROC) and the Average Precision (AP). These metrics jointly reflect the localization precision and global detection quality of generated anomalies under a consistent evaluation protocol.

Implementation Details. We adopt the pretrained Stable Diffusion v1.5 model with T=100 denoising steps and a

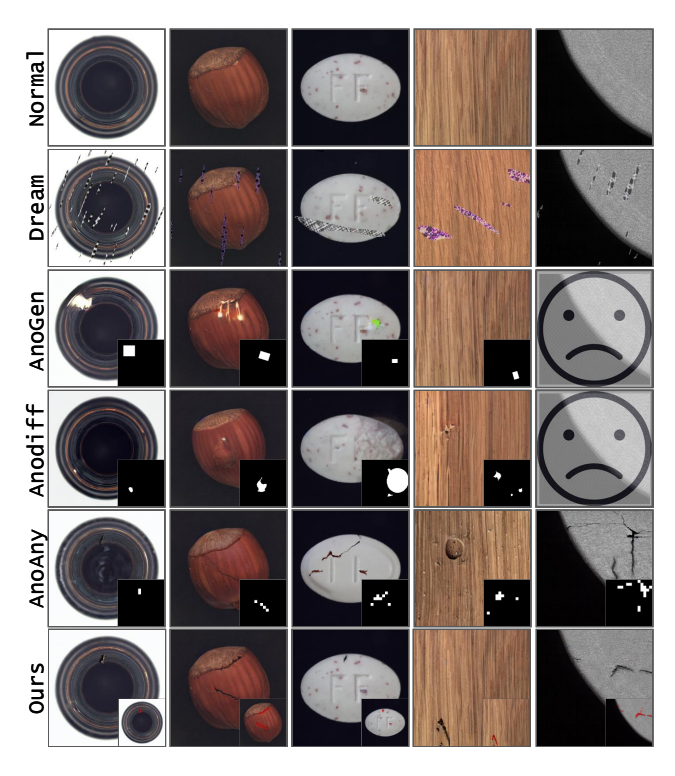


Figure 3. Qualitative comparison with existing anomaly generation methods. Columns 1–4 are MVTec AD categories; the rightmost column presents unseen categories outside MVTec AD.

partial-noise ratio of γ =0.3. During generation, we extract the mask at $t_{\rm mid}$ using a threshold of 0.6, and the final mask at the last step with a threshold of 0.35 by default. Unless otherwise stated, all other parameters and implementation settings follow the standard Stable Diffusion configuration. Additional implementation details and experiments are provided in the supplementary material.

4.2. Anomaly Generation Results

Qualitative visualization. We conduct a qualitative comparison on major MVTec AD categories and real industrial unseen categories against some existing works as shown in Fig. 3. DRAEM, due to its cut-paste composition, often shows illumination/material mismatch and boundary seams, resulting in weak photorealism. AnomalyDiffusion and AnoGen (FSAG) require few-shot fine-tuning with real defects and pixel masks. So they work on seen classes but fail to transfer to unseen classes, tending to regress toward category-specific priors. AnomalyAny broadens coverage without fine-tuning, yet its masks come from low-resolution cross-attention, yielding blurry boundaries and mislocalization or missed regions. Moreover, it re-synthesizes the entire foreground, which frequently degrades nondefect regions. In contrast, our method derives an imagespecific mask via latent-level delta-denoising and applies

mask-constrained inpainting, producing sharper, higherresolution boundaries and realistic, context-consistent defects while preserving the normal-mode appearance outside the mask in a fully training-free setting.

Generation quality. We evaluate anomaly image quality on MVTec AD using Inception Score (IS, fidelity) and IC-LPIPS (diversity) (Tab. 1). Our method achieves higher IS and IC-LPIPS than the existing works. Consistent with our qualitative results, DRAEM shows limited photorealism, and FSAG baselines (DFMGAN, Anomaly-Diffusion) rely on few-shot fine-tuning with real defects and masks, which ties synthesis to class priors and weakens cross-category generalization. AnomalyAny performs foreground-wide editing that often leaves background or clean regions inconsistent. In contrast, **DeltaDeno** achieves a balanced combination of generalization, mask precision, and photorealistic fidelity.

4.3. Anomaly Detection Results

We evaluate the effectiveness of the generated anomalous data via a downstream detection task on MVTec AD. Following prior settings, we generate 100 anomalous images per category to ensure a fair comparison and train a simple U-Net on the synthesized data. We report performance on the real MVTec AD test split (Tab. 2). For our DeltaDeno and AnomalyAny, we further control the source by generating from the same single normal image per category to isolate the generation effect. No anomalous samples from the MVTec AD are used during our synthesis or U-Net training. Note that few-shot approaches such as DFMGAN, AnomalyDiffusion, and AnoGen adapt with real defects and masks and, in some setups, use up to one-third of the test data during training. This causes data leakage and gets better anomaly detection performance. Therefore we primarily compare against AnomalyAny for ZSAG while listing DFMGAN, AnomalyDiffusion, and AnoGen as reference.

Results show that our synthesized data yield consistently higher downstream detection scores than AnomalyAny with clear gains on AUROC and AP. We also surpass DFM-GAN by a large margin and notably outperform AnoGen on P-AUROC. Overall, the gains come from jointly balancing localization precision, contextual fidelity, and morphological diversity during synthesis. Note that under the ZSAG setting the distribution of synthesized defect types inevitably differs from the real dataset. Some MVTec AD categories contain more complex or fine-grained defects, for which the detection improvement is limited or even lower. All results are obtained with the same U-Net architecture and training schedule without test-time adaptation.

4.4. Ablation Studies

We run two kinds of ablations on MVTec AD. The first is a qualitative visualization that examines generation qual-

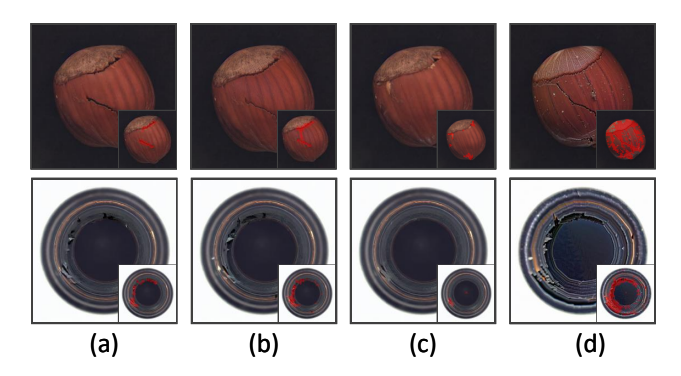


Figure 4. **Ablation visualization of main modules.** (a) *DeltaDeno* (full). (b) w/o L_{ctx} . (c) w/o spatial attention biasing. (d) w/o latent mask inpainting during late denoising stage.

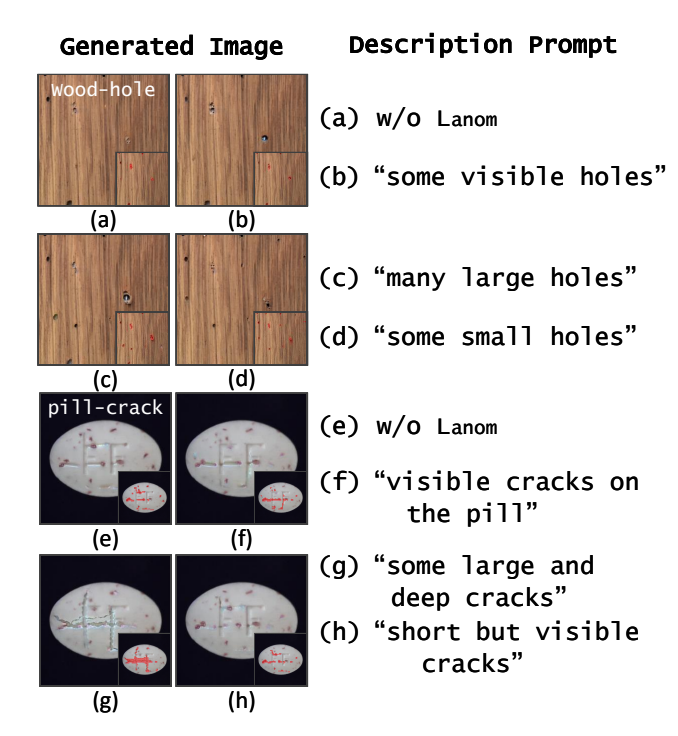


Figure 5. Ablation visualization of the Anomaly Semantic Distillation module. Varying the description prompts steers the generated defect type and severity, yielding more controllable and diverse anomalies.

ity and localization. The second is a downstream detection study that measures practical utility. The ablated parts include three modules: *latent-mask inpainting* (A), *spatial attention biasing* (B), and *token-level prompt refinement* (C, implemented with \mathcal{L}_{ctx} and $\mathcal{L}_{\text{anom}}$). We also visualize how the descriptive anchor in $\mathcal{L}_{\text{anom}}$ affects the result.

For the visualization protocol, each category synthesizes the same number of anomalies from the same normal guidance image with matched seeds and schedule (Fig. 4). *Latent-mask inpainting* keeps edits strictly inside the mask

Table 3. **Ablation on downstream detection (mean %).** Higher is better. A: latent-mask inpainting, B: attention biasing, C: prompt refinement.

Method	$AUC_i \uparrow$	$AP_i \uparrow$	$\mathrm{AUC}_p\uparrow$	$AP_p \uparrow$
w/o A	79.7	87.6	81.2	25.8
w/o B	79.5	88.2	83.4	28.3
w/o C	78.8	86.3	83.1	28.1
DeltaDeno (full)	84.7	91.3	84.9	30.5

so non-defect regions preserve geometry and illumination, which yields coherent backgrounds. Spatial attention biasing strengthens the cross-attention of the anomaly token inside the mask, which improves semantic faithfulness, sharpens boundaries, and increases the contrast between the two synchronized trajectories. The prompt refinement loss \mathcal{L}_{ctx} stabilizes the semantics of non-anomaly tokens, which suppresses off-target drift and aligns the visible difference with the true defect area. In addition, the semantic distillation term \mathcal{L}_{anom} turns the description into a controllable anchor. Changing the description such as length, width, texture, or depth steers the defect morphology and increases sample diversity while latent-mask inpainting preserves background fidelity (Fig. 5).

For downstream detection, all variants follow the same protocol. In each category we synthesize an equal number of anomalies from the same normal guidance image. A single U-Net is trained on each generated set and evaluated on MVTec AD, and we report image-level and pixel-level AUROC and AP (Tab. 3). The results agree with the visual ablations. The full configuration reaches the highest AUROC and AP. Removing any one of modules produces a clear drop, and the trend is stable across categories.

5. Conclusion

We introduced DeltaDeno, a training-free zero-shot anomaly generation framework that leverages deltadenoising to localize and edit defects in a normal sample. By contrasting two synchronized diffusion branches conditioned on normal and anomaly prompts, the method derives reliable masks and performs mask-guided latent inpainting to synthesize photorealistic, context-consistent anomalies. A normal-reference initialization keeps synthesis aligned with the distribution of normal content, while lightweight prompt refinement with spatially biased attention stabilizes localization without retraining. On public benchmarks, DeltaDeno attains higher generation quality and stronger downstream detection performance. The framework requires no anomalous labels or model adaptation and is practical for rapid data bootstrapping and stress testing when real defects are scarce.

Limitations and Future Work. Despite its effectiveness,

DeltaDeno still faces several limitations. First, existing evaluation protocols for ZSAG are limited and may require MLLM-based comprehensive assessment in the future. Second, the controllability offered by semantic distillation remains limited, constraining fine-grained manipulation of defect attributes. Third, most generated anomalies exhibit structural or surface-level characteristics, while more abstract or logical defects remain challenging to produce. Future work can investigate these unresolved aspects to further improve the capability of zero-shot anomaly generation.

References

- [1] Omri Avrahami, Ohad Fried, and Dani Lischinski. Blended latent diffusion. *ACM transactions on graphics (TOG)*, 42 (4):1–11, 2023. 2
- [2] Paul Bergmann, Michael Fauser, David Sattlegger, and Carsten Steger. Mytec ad–a comprehensive real-world dataset for unsupervised anomaly detection. In *Proceedings* of the IEEE/CVF conference on computer vision and pattern recognition, pages 9592–9600, 2019. 1, 6
- [3] Paul Bergmann, Michael Fauser, David Sattlegger, and Carsten Steger. Uninformed students: Student-teacher anomaly detection with discriminative latent embeddings. In Proceedings of the IEEE/CVF conference on computer vision and pattern recognition, pages 4183–4192, 2020. 1
- [4] Tim Brooks, Aleksander Holynski, and Alexei A Efros. Instructpix2pix: Learning to follow image editing instructions. In *Proceedings of the IEEE/CVF conference on computer vi*sion and pattern recognition, pages 18392–18402, 2023. 2
- [5] Mingdeng Cao, Xintao Wang, Zhongang Qi, Ying Shan, Xi-aohu Qie, and Yinqiang Zheng. Masactrl: Tuning-free mutual self-attention control for consistent image synthesis and editing. In *Proceedings of the IEEE/CVF international conference on computer vision*, pages 22560–22570, 2023. 2
- [6] Hila Chefer, Yuval Alaluf, Yael Vinker, Lior Wolf, and Daniel Cohen-Or. Attend-and-excite: Attention-based semantic guidance for text-to-image diffusion models. ACM transactions on Graphics (TOG), 42(4):1–10, 2023. 2
- [7] Qiyu Chen, Huiyuan Luo, Chengkan Lv, and Zhengtao Zhang. A unified anomaly synthesis strategy with gradient ascent for industrial anomaly detection and localization. In *European Conference on Computer Vision*, pages 37–54. Springer, 2024. 1
- [8] Qiyu Chen, Huiyuan Luo, Haiming Yao, Wei Luo, Zhen Qu, Chengkan Lv, and Zhengtao Zhang. Center-aware residual anomaly synthesis for multiclass industrial anomaly detection. *IEEE Transactions on Industrial Informatics*, 21(9): 7276–7286, 2025. 1
- [9] Guillaume Couairon, Jakob Verbeek, Holger Schwenk, and Matthieu Cord. Diffedit: Diffusion-based semantic image editing with mask guidance. *arXiv preprint arXiv:2210.11427*, 2022. 2
- [10] Zhewei Dai, Shilei Zeng, Haotian Liu, Xurui Li, Feng Xue, and Yu Zhou. Seas: few-shot industrial anomaly image generation with separation and sharing fine-tuning. In *Proceed*-

- ings of the IEEE/CVF International Conference on Computer Vision, pages 23135–23144, 2025. 1, 3, 6
- [11] Prafulla Dhariwal and Alexander Nichol. Diffusion models beat gans on image synthesis. *Advances in neural information processing systems*, 34:8780–8794, 2021. 1
- [12] Yuxuan Duan, Yan Hong, Li Niu, and Liqing Zhang. Fewshot defect image generation via defect-aware feature manipulation. In *Proceedings of the AAAI conference on artificial intelligence*, pages 571–578, 2023. 1, 3, 6
- [13] Qingqing Fang, Qinliang Su, Wenxi Lv, Wenchao Xu, and Jianxing Yu. Boosting fine-grained visual anomaly detection with coarse-knowledge-aware adversarial learning. In *Proceedings of the AAAI Conference on Artificial Intelligence*, pages 16532–16540, 2025. 1
- [14] Guan Gui, Bin-Bin Gao, Jun Liu, Chengjie Wang, and Yunsheng Wu. Few-shot anomaly-driven generation for anomaly classification and segmentation. In *European Conference on Computer Vision*, pages 210–226. Springer, 2024. 6
- [15] Amir Hertz, Ron Mokady, Jay Tenenbaum, Kfir Aberman, Yael Pritch, and Daniel Cohen-Or. Prompt-to-prompt image editing with cross attention control. *arXiv preprint arXiv:2208.01626*, 2022. 2
- [16] Jonathan Ho and Tim Salimans. Classifier-free diffusion guidance. *arXiv preprint arXiv:2207.12598*, 2022. 1
- [17] Jonathan Ho, Ajay Jain, and Pieter Abbeel. Denoising diffusion probabilistic models. Advances in neural information processing systems, 33:6840–6851, 2020. 1
- [18] Teng Hu, Jiangning Zhang, Ran Yi, Yuzhen Du, Xu Chen, Liang Liu, Yabiao Wang, and Chengjie Wang. Anomalydiffusion: Few-shot anomaly image generation with diffusion model. In *Proceedings of the AAAI conference on artificial intelligence*, pages 8526–8534, 2024. 1, 3, 6
- [19] Ying Jin, Jinlong Peng, Qingdong He, Teng Hu, Jiafu Wu, Hao Chen, Haoxuan Wang, Wenbing Zhu, Mingmin Chi, Jun Liu, et al. Dual-interrelated diffusion model for few-shot anomaly image generation. In *Proceedings of the Computer Vision and Pattern Recognition Conference*, pages 30420–30429, 2025. 1, 3, 6
- [20] Bahjat Kawar, Shiran Zada, Oran Lang, Omer Tov, Huiwen Chang, Tali Dekel, Inbar Mosseri, and Michal Irani. Imagic: Text-based real image editing with diffusion models. In Proceedings of the IEEE/CVF conference on computer vision and pattern recognition, pages 6007–6017, 2023. 2
- [21] Diederik P Kingma and Max Welling. Auto-encoding variational bayes. *arXiv preprint arXiv:1312.6114*, 2013. 3
- [22] Alexander Kirillov, Eric Mintun, Nikhila Ravi, Hanzi Mao, Chloe Rolland, Laura Gustafson, Tete Xiao, Spencer Whitehead, Alexander C Berg, Wan-Yen Lo, et al. Segment anything. In *Proceedings of the IEEE/CVF international conference on computer vision*, pages 4015–4026, 2023. 5
- [23] Chun-Liang Li, Kihyuk Sohn, Jinsung Yoon, and Tomas Pfister. Cutpaste: Self-supervised learning for anomaly detection and localization. In *Proceedings of the IEEE/CVF conference on computer vision and pattern recognition*, pages 9664–9674, 2021. 1
- [24] Dongyun Lin, Yanpeng Cao, Wenbin Zhu, and Yiqun Li. Few-shot defect segmentation leveraging abundant defect-

- free training samples through normal background regularization and crop-and-paste operation. In 2021 IEEE International Conference on Multimedia and Expo (ICME), pages 1–6. IEEE Computer Society, 2021. 1, 6
- [25] Chenlin Meng, Yutong He, Yang Song, Jiaming Song, Jiajun Wu, Jun-Yan Zhu, and Stefano Ermon. Sdedit: Guided image synthesis and editing with stochastic differential equations. arXiv preprint arXiv:2108.01073, 2021. 2
- [26] Ron Mokady, Amir Hertz, Kfir Aberman, Yael Pritch, and Daniel Cohen-Or. Null-text inversion for editing real images using guided diffusion models. In *Proceedings of* the IEEE/CVF conference on computer vision and pattern recognition, pages 6038–6047, 2023. 2
- [27] Alexander Quinn Nichol and Prafulla Dhariwal. Improved denoising diffusion probabilistic models. In *International* conference on machine learning, pages 8162–8171. PMLR, 2021. 1
- [28] Zhen Qu, Xian Tao, Fei Shen, Zhengtao Zhang, and Tao Li. Investigating shift equivalence of convolutional neural networks in industrial defect segmentation. *IEEE Transactions* on *Instrumentation and Measurement*, 72:1–17, 2023. 1
- [29] Robin Rombach, Andreas Blattmann, Dominik Lorenz, Patrick Esser, and Björn Ommer. High-resolution image synthesis with latent diffusion models. In *Proceedings of* the IEEE/CVF conference on computer vision and pattern recognition, pages 10684–10695, 2022. 1, 2
- [30] Olaf Ronneberger, Philipp Fischer, and Thomas Brox. Unet: Convolutional networks for biomedical image segmentation. In *International Conference on Medical image computing and computer-assisted intervention*, pages 234–241. Springer, 2015. 3
- [31] Qingfeng Shi, Jing Wei, Fei Shen, and Zhengtao Zhang. Few-shot defect image generation based on consistency modeling. In *European Conference on Computer Vision*, pages 360–376. Springer, 2024. 1
- [32] Jiaming Song, Chenlin Meng, and Stefano Ermon. Denoising diffusion implicit models. arXiv preprint arXiv:2010.02502, 2020. 4
- [33] Jaewoo Song, Daemin Park, Kanghyun Baek, Sangyub Lee, Jooyoung Choi, Eunji Kim, and Sungroh Yoon. Defectfill: Realistic defect generation with inpainting diffusion model for visual inspection. In Proceedings of the Computer Vision and Pattern Recognition Conference, pages 18718–18727, 2025. 1, 6
- [34] Han Sun, Yunkang Cao, Hao Dong, and Olga Fink. Unseen visual anomaly generation. In *Proceedings of the Computer Vision and Pattern Recognition Conference*, pages 25508– 25517, 2025. 1, 3, 6
- [35] Vitjan Zavrtanik, Matej Kristan, and Danijel Skočaj. Draema discriminatively trained reconstruction embedding for surface anomaly detection. In *Proceedings of the IEEE/CVF international conference on computer vision*, pages 8330–8339, 2021. 1, 3, 6
- [36] Gongjie Zhang, Kaiwen Cui, Tzu-Yi Hung, and Shijian Lu. Defect-gan: High-fidelity defect synthesis for automated defect inspection. In *Proceedings of the IEEE/CVF Win*ter Conference on Applications of Computer Vision, pages 2524–2534, 2021. 1, 3

[37] Qihang Zhou, Guansong Pang, Yu Tian, Shibo He, and Jiming Chen. Anomalyclip: Object-agnostic prompt learning for zero-shot anomaly detection. In *International Conference on Learning Representations*, 2024. 1